

Instability of nanofluid film flow under external electric field: Linear and weakly nonlinear analysis

Xinshan Li(李欣珊), Danting Xue(薛丹婷), Ruigang Zhang(张瑞岗), Quansheng Liu(刘全生), and Zhaodong Ding(丁兆东)

Citation: Chin. Phys. B, 2025, 34 (**12**): 124701. DOI: 10.1088/1674-1056/addcc0
http://cpb.iphy.ac.cn; http://iopscience.iop.org/cpb

What follows is a list of articles you may be interested in

Neural network analysis for prediction of heat transfer of aqueous hybrid nanofluid flow in a variable porous space with varying film thickness over a stretched surface

Abeer S Alnahdi and Taza Gul
Chin. Phys. B, 2025, 34 (**2**): 024701. DOI: 10.1088/1674-1056/ad989c

Casson hybrid nanofluid flow over a Riga plate for drug delivery applications with double diffusion

Abeer S. Alnahdi and Taza Gul
Chin. Phys. B, 2024, 33 (**10**): 104701. DOI: 10.1088/1674-1056/ad624e

Rayleigh-Taylor instability of viscoelastic self-rewetting film flowing down a temperature-controlled inclined substrate

Siyi An(安思亦) and Yongjun Jian(菅永军)
Chin. Phys. B, 2023, 32 (**6**): 064701. DOI: 10.1088/1674-1056/acc78b

Physical aspects of magnetized Jeffrey nanomaterial flow with irreversibility analysis

Fazal Haq, Muhammad Ijaz Khan, Sami Ullah Khan, Khadijah M Abualnaja, and M A El-Shorbagy
Chin. Phys. B, 2022, 31 (**8**): 084703. DOI: 10.1088/1674-1056/ac4236

Influence of various shapes of nanoparticles on unsteady stagnation-point flow of Cu-H_2O nanofluid on a flat surface in a porous medium: A stability analysis

Astick Banerjee, Krishnendu Bhattacharyya, Sanat Kumar Mahato, and Ali J. Chamkha
Chin. Phys. B, 2022, 31 (**4**): 044701. DOI: 10.1088/1674-1056/ac229b

---

Instability of nanofluid film flow under external electric field: Linear and weakly nonlinear analysis

Xinshan Li(李欣珊), Danting Xue(薛丹婷), Ruigang Zhang(张瑞岗), Quansheng Liu(刘全生), and Zhaodong Ding(丁兆东)†

School of Mathematical Sciences, Inner Mongolia University, Hohhot 010021, *China*

(Received 29 March 2025; revised manuscript received 4 May 2025; accepted manuscript online 23 May 2025)

This study investigates the instability of nanofluid thin films flowing down an inclined plane under the influence of a normal electric field. Based on the long-wave approximation and a systematic asymptotic expansion, a nonlinear evolution equation is derived to capture the coupled effects of the electric field and nanoparticle properties. Linear stability analysis reveals that the electric field enhances interfacial disturbances and promotes instability, whereas the presence of nanoparticles suppresses this effect by attenuating disturbance amplitudes. A weakly nonlinear analysis further clarifies the interplay among electric field strength, nanoparticle volume fraction, and density difference, enabling a classification of nonlinear stability regimes. Numerical simulations support the analytical predictions, showing that in unstable regimes, perturbations grow over time and eventually destabilize the film. These findings offer theoretical insights into the control of nanofluid film stability via electric field regulation and nanoparticle tuning.

Keywords: thin film instability, nonlinear evolution equation, nanofluid

PACS: 47.20.Dr, 47.11.St, 47.10.A–

DOI: 10.1088/1674-1056/addcc0 **CSTR:** 32038.14.CPB.addcc0

1. Introduction

Liquid film flow refers to the phenomenon where a liquid forms a thin layer and flows along a substrate surface.[1–4] Its stability is influenced by a variety of factors, including gravity, surface tension, electric fields, and thermal capillary forces.[5–13] In most cases, liquid film flow is gravity-driven, with the liquid flowing along inclined or vertical surfaces under the influence of gravity, forming a stable film.[1,6,14] However, by applying a temperature or concentration gradient,[5,8,15] an interfacial tension gradient can be generated, significantly altering the stability of the liquid film and leading to instability.[9,12] Additionally, the external force fields applied, such as electric or magnetic fields, can also contribute to film instability.[6,10] Liquid film flow has important applications in various areas.[4,16,17] In chemical engineering, liquid films are used for gas separation and seawater desalination; in heat exchange, liquid films improve heat transfer efficiency; in coating manufacturing, liquid film technology is employed for the production of high-quality films; and in biomedical and food industries, liquid films are used for food preservation, among other applications.[8,18–22] A deeper understanding of the stability mechanisms of liquid film flow helps ensure its efficiency, energy-saving potential, and environmental sustainability in practical applications, making it an important technological support for modern industries and scientific research.

The interfacial stability of liquid films is a fundamental topic in fluid mechanics, with significant contributions from Benjamin[1] and Yih.[2,2] Their pioneering studies identified the critical Reynolds number, below which film flow transitions from stable to unstable due to gravitational forces. Building on this foundation, Benney[23] introduced finite amplitude stability analysis, deriving the now-famous Benney equation using a perturbation expansion with long-wave approximations. This equation provided a framework for analyzing the nonlinear dynamics of film flow. Further advancements[24–27] employed weakly nonlinear analysis to deepen the understanding of film stability. More later works, such as those by Kondic,[28] Banerjee *et al.*,[29] and Bauer and Kerczek,[30] have extended these insights, exploring the complex stability characteristics of thin films on inclined and vertical surfaces. Together, these studies form the foundation for modern research into the intricate behavior of liquid film flows under varying conditions. Recently, the stability of liquid films has still received widespread attention. Zhang and Ding[31] investigated the effects of surfactants on the surface capillary waves of liquid films at the nanoscale. They explored how surfactants alter the time dependence of surface tension and elasticity and revealed the influence of surface viscosity on thermal capillary waves. Hu[13] investigated the nonlinear waves in a shear liquid film in a horizontal plane by theoretical analysis and numerical simulation. They explored the effects of surface ten-

†Corresponding author. E-mail: dingzhd@imu.edu.cn

© 2025 Chinese Physical Society and IOP Publishing Ltd. All rights, including for text and data mining, AI training, and similar technologies, are reserved.

sion and gravity on the stability of the film, and revealed the evolution characteristics of solitary and periodic waves in the liquid film. Their work highlighted the role of surface tension and gravity in film stability and provided insights into the evolution of solitary and periodic waves in liquid films.

In practical applications, the study of nanofluid flows has gained significant attention, particularly for their enhanced heat transfer properties. Nanofluids, which are two-phase mixtures of a liquid base fluid and ultrafine nanoscale particles, are widely utilized for applications requiring efficient thermal management. For example, a low concentration of particles can enhance heat transfer.[32–34] Nanofluids are two-phase mixtures typically comprising a liquid as the basic fluid and ultrafine nanoscale particles. Research by Nayak *et al.*[35] has demonstrated that the flow stability of nanofluids is enhanced, with the degree of suppression varying depending on the concentration of nanoparticles.[36] Lin *et al.*[37] investigated the linear instability of nanofluid flow in channels. They applied instability theory to derive control equations featuring average particle mass load, average Stokes number, Reynolds number, and Knudsen number, and obtained numerical solutions for these equations. The results suggested that nanoparticles suppress instability, though they do not entirely eliminate it. The instability can be altered by increasing the particle mass load. Dero *et al.*[38] explored the flow of micropolar nanofluids over permeable stretching and shrinking surfaces, identifying dual solutions for certain parameters and determining their stability. Lin and Yang[39] briefly reviewed the achievements in research on nanofluid flow instability, including hydrodynamic and thermal instability. Studying the stability of nanofluid films is crucial for exploring their applications in engineering.

Moreover, film flow and its interactions with electric fields have broad applications across various engineering fields. The introduction of an electric field generates additional interfacial stress, thereby influencing the stability of the flow.[40,41] Gonzalez and Castellanos[42] studied the stability of thin film flow down an inclined plane under the influence of an electric field and derived a nonlinear evolution equation. Tseluiko *et al.*[43] used a long-wave approximation to study the effects of a normal electric field on a falling film, finding that electric fields can destabilize the flow. Samanta[44] investigated the linear stability of viscous film flow over an oscillating plane, revealing that the presence of an electric field expands the unstable wave number region. Uma and Usha[45] examined the temporal evolution of thin conductive liquid films flowing down a porous inclined substrate when the electric field is perpendicular to the substrate. They analyzed the resulting nonlinear evolution equation from both linear stability and weakly nonlinear stability perspectives, demonstrating that electric fields promote instability in liquid film flow.

Although significant advances have been made in studying the effects of electric fields on conventional liquid films, research on nanofluid films remains limited, particularly regarding the role of nanoparticle properties such as volume fraction and density difference. Moreover, previous studies rarely derived nonlinear evolution equations that couple nanoparticle effects with electric fields. This work addresses these gaps by examining the instability of nanofluid thin films descending an inclined plane under an external electric field. The main contributions are: (i) introducing the effect of nanoparticle density contrast on flow stability; (ii) deriving a nonlinear evolution equation coupling electric field and nanoparticle influences; and (iii) proposing a multi-parameter classification of nonlinear stability regimes based on electric field intensity, nanoparticle volume fraction, and density difference. These findings offer new insights into the interplay between electric fields and nanoparticles in film flow stability.

2. Mathematical model

We investigate the flow of an incompressible, viscous nanofluid film down an inclined surface under the influence of gravity g and an electric field E in a two-dimensional (2D) space. Examples of such nanofluid thin films include nanoparticle-laden coatings used in heat-dissipating layers for microelectronic cooling systems, nanofluid films in lab-on-a-chip devices where electric fields are used for flow control, and electrically responsive functional films designed for applications in microgravity environments such as spacecraft thermal management. In these systems, electric fields are often employed to manipulate film behavior, while the addition of nanoparticles is known to enhance thermal conductivity, modify interfacial properties, and affect flow stability.[46] However, in the present study, the thermal conductivity enhancement is not considered, as the focus is placed on interfacial dynamics and hydrodynamic stability. The model schematic is shown in Fig. 1. The Cartesian coordinate system (x,y) forms an angle β with the horizontal plane. The free surface is given by $y = h(x,t)$, where h_0 represents the unperturbed film thickness. Two rigid, parallel electrodes, separated by distance d, bound the film: the lower plate at $y = 0$ is held at constant potential $\varphi_1 = \varphi_c$, and the upper plate at $y = d$ is grounded ($\varphi_2 = 0$). To make the problem tractable, we invoke the following approximations: (i) Longwave (lubrication) approximation, the average liquid film thickness and wavelength satisfy $\alpha = h_0/\lambda \ll 1$, allowing an asymptotic expansion in α. (ii) Region 1 (nanofluid) is an incompressible, Newtonian conductor with uniformly dispersed, neutrally wetted nanoparticles; region 2 is an ideal, chargefree dielectric with permit-

tivity ε_0. (iii) Quasielectrostatic limit, magnetic effects, and displacement currents are neglected, so that $\boldsymbol{E} = -\nabla\varphi$, with φ satisfying Laplace' equation in each region. (iv) Ideal conductor approximation, the nanofluid bulk potential is uniform, confining electric-field gradients to the dielectric layer; any field effect within the fluid region itself is neglected.

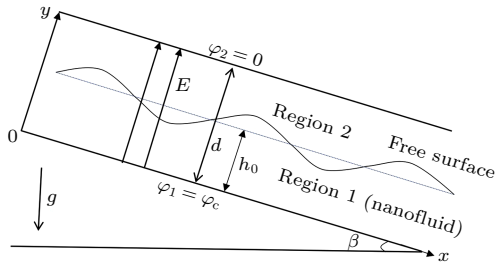


Fig. 1. The schematic diagram of the physical model.

In region 1 (the nanofluid domain), the flow is governed by the continuity and momentum equations under the incompressible Newtonian fluid assumption. The velocity field in the inclined Cartesian coordinate system is denoted by $\boldsymbol{u} = (u, v)$, where u and v represent the velocity components along the x- and y-directions, respectively. The continuity equation, ensuring mass conservation, is given by

$$\frac{\partial u}{\partial x} + \frac{\partial v}{\partial y} = 0. \tag{1}$$

The momentum equations along the x- and y-directions respectively describe the balance between inertial, pressure, gravitational, and viscous forces in the film

$$\begin{aligned} &\rho_{\mathrm{f}}\left(\frac{\partial u}{\partial t} + u\frac{\partial u}{\partial x} + v\frac{\partial u}{\partial y}\right) \\ &= -\frac{\partial p}{\partial x} + \rho_{\mathrm{n}} g\sin\beta + \mu_{\mathrm{n}}\left(\frac{\partial^2 u}{\partial x^2} + \frac{\partial^2 u}{\partial y^2}\right), \end{aligned} \tag{2}$$

$$\begin{aligned} &\rho_{\mathrm{f}}\left(\frac{\partial v}{\partial t} + u\frac{\partial v}{\partial x} + v\frac{\partial v}{\partial y}\right) \\ &= -\frac{\partial p}{\partial y} - \rho_{\mathrm{n}} g\cos\beta + \mu_{\mathrm{n}}\left(\frac{\partial^2 v}{\partial x^2} + \frac{\partial^2 v}{\partial y^2}\right). \end{aligned} \tag{3}$$

Here, ρ_{f} is the density of the base fluid, ρ_{n} is the density of the nanofluid, and μ_{n} is the viscosity coefficient of the nanofluid.[47] The inclusion of ρ_{n} instead of ρ_{f} in the gravity terms accounts for the effect of nanoparticle loading on the effective fluid density. To describe the transport of nanoparticles, we assume the particles are uniformly dispersed and follow the flow without phase separation. Their distribution is governed by a convection equation for the local volume fraction ϕ:

$$\frac{\partial \phi}{\partial t} + u\frac{\partial \phi}{\partial x} + v\frac{\partial \phi}{\partial y} = 0. \tag{4}$$

In region 2 (above the film), which is treated as a quiescent, charge-free dielectric medium with permittivity ε_0, the electric field is purely electrostatic and defined by the potential gradient

$$\boldsymbol{E}_2 = -\nabla\varphi_2, \tag{5}$$

where φ_2 satisfies Laplace's equation due to the absence of free charges

$$\frac{\partial^2 \varphi_2}{\partial x^2} + \frac{\partial^2 \varphi_2}{\partial y^2} = 0. \tag{6}$$

At the bottom plate $y = 0$, the boundary conditions for fluid no-slip and no-penetration are

$$u = v = 0. \tag{7}$$

Since the nanoparticles cannot penetrate the wall, the diffusion flux on the wall should be zero, and it can be expressed as

$$\frac{\partial \phi}{\partial y} = 0. \tag{8}$$

At the free surface $y = h(x,t)$, the behavior of the interface is governed by a combination of kinematic, dynamic (normal and tangential stress), and electrostatic boundary conditions. These conditions ensure the consistency of fluid motion, force balance, and electric potential across the deformable interface. First, the tangential stress condition at the interface ensures the balance of viscous shear stresses along the inclined surface. It can be written as

$$\left[1 - \left(\frac{\partial h}{\partial x}\right)^2\right]\left(\frac{\partial u}{\partial y} + \frac{\partial v}{\partial x}\right) - 4\frac{\partial h}{\partial x}\frac{\partial u}{\partial x} = 0. \tag{9}$$

The normal stress condition expresses the balance between hydrodynamic pressure, viscous normal stress, capillary pressure due to surface tension, and electric normal stresses. It is expressed as follows:

$$\begin{aligned} &p_a - p + \frac{\mu_{\mathrm{n}}}{1 + \left(\frac{\partial h}{\partial x}\right)^2}\left\{2\frac{\partial v}{\partial y}\left[1 - \left(\frac{\partial h}{\partial x}\right)^2\right]\right. \\ &\left. -2\frac{\partial h}{\partial x}\left(\frac{\partial u}{\partial y} + \frac{\partial v}{\partial x}\right)\right\} \\ &= \frac{\sigma_0 \frac{\partial^2 h}{\partial x^2}}{\left[1 + \left(\frac{\partial h}{\partial x}\right)^2\right]^{3/2}} + \frac{\varepsilon_0}{1 + \left(\frac{\partial h}{\partial x}\right)^2}\left(\frac{\partial h}{\partial x}\frac{\partial \varphi_2}{\partial x} - \frac{\partial \varphi_2}{\partial y}\right)^2 \\ &- \frac{\varepsilon_0}{2}\left[\left(\frac{\partial \varphi_2}{\partial x}\right)^2 + \left(\frac{\partial \varphi_2}{\partial y}\right)^2\right]. \end{aligned} \tag{10}$$

On the left-hand side, the pressure inside the fluid is modified by viscous effects; on the right-hand side, the first term accounts for surface tension (capillary pressure), while the remaining terms represent Maxwell stresses from the electric field in the dielectric layer above the film. The kinematic

boundary condition ensures that the free surface moves with the fluid

$$\frac{\partial h}{\partial t}+u\frac{\partial h}{\partial x}-v=0. \tag{11}$$

Regarding the electrostatic boundary conditions, continuity of electric potential is imposed at the free surface. Since the nanofluid is modeled as an ideal conductor, the potential remains constant throughout the fluid and at the interface

$$\varphi_2\mid_{y=h}=\varphi_1\mid_{y=h}=\varphi_{\rm c}. \tag{12}$$

At the upper electrode ($y=d$), which is grounded, the electric potential is zero

$$\varphi_2\mid_{y=d}=0. \tag{13}$$

These conditions define a uniform potential drop across the dielectric region, leading to a vertical electric field in the undisturbed state.

Based on the modeling assumptions, we proceed to simplify the governing equations using lubrication theory, which is valid in the long-wave limit. Specifically, we assume that the characteristic wavelength of interface deformation λ is much larger than the undisturbed film thickness h_0, such that the film parameter $\alpha=h_0/\lambda\ll 1$. This allows for an asymptotic expansion in terms of α, significantly reducing the complexity of the governing equations. To further nondimensionalize the system, we introduce the following characteristic scales and define the corresponding dimensionless variables (denoted with a superscript asterisk)

$$\begin{aligned}
&x^*=\frac{\alpha x}{h_0},\quad h^*=\frac{h}{h_0},\quad y^*=\frac{y}{h_0},\\
&t^*=\frac{\alpha U_0 t}{h_0},\quad d^*=\frac{d}{h_0},\quad u^*=\frac{u}{U_0},\\
&v^*=\frac{v}{\alpha U_0},\quad p^*=\frac{p}{\mu_{\rm f}U_0/h_0},\\
&\varphi^*=\frac{\varphi}{\varphi_{\rm c}},\quad \phi^*=\frac{\phi}{\phi_{\rm ave}},
\end{aligned} \tag{14}$$

where $U_0=\rho_{\rm f}gh_0^2\sin\beta/3\mu_{\rm f}$ is the base velocity, $\mu_{\rm f}$ is the viscosity coefficient of the base fluid, and $\phi_{\rm ave}$ is the average volume fraction of nanoparticles over a certain period.

These scalings transform the governing equations and boundary conditions into a dimensionless form, enabling the relative importance of inertia, gravity, viscosity, and electric forces to be captured through key dimensionless groups such as the Reynolds number, capillary number, and electric field strength. By substituting the non-dimensional variables into the equations and omitting the asterisks for clarity, the resulting dimensionless equations in region 1 are given by

$$\frac{\partial u}{\partial x}+\frac{\partial v}{\partial y}=0, \tag{15}$$

$$\begin{aligned}
&\alpha Re\left(\frac{\partial u}{\partial t}+u\frac{\partial u}{\partial x}+v\frac{\partial u}{\partial y}\right)\\
&=-\alpha\frac{\partial p}{\partial x}+3F_\rho+F_\mu\left(\alpha^2\frac{\partial^2 u}{\partial x^2}+\frac{\partial^2 u}{\partial y^2}\right),
\end{aligned} \tag{16}$$

$$\begin{aligned}
&\alpha^2 Re\left(\frac{\partial v}{\partial t}+u\frac{\partial v}{\partial x}+v\frac{\partial v}{\partial y}\right)\\
&=-\frac{\partial p}{\partial y}-3F_\rho\cot\beta+F_\mu\left(\alpha^3\frac{\partial^2 v}{\partial x^2}+\alpha\frac{\partial^2 v}{\partial y^2}\right),
\end{aligned} \tag{17}$$

$$\frac{\partial \phi}{\partial t}+u\frac{\partial \phi}{\partial x}+v\frac{\partial \phi}{\partial y}=0. \tag{18}$$

In region 2, the dimensionless electric potential satisfies Laplace's equation

$$\alpha^2\frac{\partial^2\varphi_2}{\partial x^2}+\frac{\partial^2\varphi_2}{\partial y^2}=0. \tag{19}$$

At the inclined bottom plate $y=0$, no-slip and impermeability conditions

$$u=v=0, \tag{20}$$

$$\frac{\partial \phi}{\partial y}=0. \tag{21}$$

At the inclined top plate $y=d$, the electric potential is grounded

$$\varphi_2=0. \tag{22}$$

At the free surface $y=h(x,t)$, the boundary conditions include

$$\left[1-\alpha^2\left(\frac{\partial h}{\partial x}\right)^2\right]\left(\frac{\partial u}{\partial y}+\alpha^2\frac{\partial v}{\partial x}\right)-4\alpha^2\frac{\partial h}{\partial x}\frac{\partial u}{\partial x}=0, \tag{23}$$

$$\begin{aligned}
&\overline{p}_{\rm a}-p+\frac{F_\mu}{1+\alpha^2\left(\frac{\partial h}{\partial x}\right)^2}\left\{2\alpha\frac{\partial v}{\partial y}\left[1-\alpha^2\left(\frac{\partial h}{\partial x}\right)^2\right]\right.\\
&\left.-2\alpha\frac{\partial h}{\partial x}\left(\frac{\partial u}{\partial y}+\alpha^2\frac{\partial v}{\partial x}\right)\right\}\\
&=\frac{\frac{\partial^2 h}{\partial x^2}}{Ca'\left[1+\alpha^2\left(\frac{\partial h}{\partial x}\right)^2\right]^{3/2}}-E\left[\alpha^2\left(\frac{\partial\varphi_2}{\partial x}\right)^2+\left(\frac{\partial\varphi_2}{\partial y}\right)^2\right]\\
&+\frac{2E}{1+\alpha^2\left(\frac{\partial h}{\partial x}\right)^2}\left(\alpha^2\frac{\partial h}{\partial x}\frac{\partial\varphi_2}{\partial x}-\frac{\partial\varphi_2}{\partial y}\right)^2,
\end{aligned} \tag{24}$$

$$\frac{\partial h}{\partial t}+u\frac{\partial h}{\partial x}-v=0, \tag{25}$$

$$\varphi_2=1, \tag{26}$$

where $\overline{p}_{\rm a}=p_{\rm a}/\rho_{\rm f}{U_0}^2$, the relative density and viscosity of the nanofluid are $F_\rho=\rho_{\rm n}/\rho_{\rm f}$ and $F_\mu=\mu_{\rm n}/\mu_{\rm f}$. The nondimensional parameters are the Reynolds number Re, the capillary nunmber Ca' and the electrical parameter E. They are expressed as

$$Re=\frac{\rho_{\rm f}U_0h_0}{\mu_{\rm f}},\quad Ca'=\frac{Ca}{\alpha^2}=\frac{\mu_{\rm f}U_0}{\alpha^2\sigma_0},\quad E=\frac{\varepsilon_0\varphi_{\rm c}^2}{2\mu_{\rm f}U_0h_0}.$$

3. Approximate solution of the equations

The physical quantities u, v, p, and φ_2 are expanded as power series of the small parameter α

$$\begin{aligned} u &= u_0 + \alpha u_1 + \cdots, \\ v &= v_0 + \alpha v_1 + \cdots, \\ p &= p_0 + \alpha p_1 + \cdots, \\ \varphi_2 &= \varphi_{20} + \alpha \varphi_{21} + \cdots. \end{aligned} \tag{27}$$

By substituting Eq. (27) into the dimensionless Eqs. (15)–(26), we obtain the zeroth-order governing equations and boundary conditions

$$\frac{\partial u_0}{\partial x} + \frac{\partial v_0}{\partial y} = 0, \tag{28}$$

$$F_\mu \frac{\partial^2 u_0}{\partial y^2} + 3F_\rho = 0, \tag{29}$$

$$Re\frac{\partial p_0}{\partial y} + 3F_\rho \cot\beta = 0, \tag{30}$$

$$\frac{\partial \phi_0}{\partial t} + u_0\frac{\partial \phi_0}{\partial x} + v_0\frac{\partial \phi_0}{\partial y} = 0, \tag{31}$$

$$\frac{\partial^2 \varphi_{20}}{\partial y^2} = 0. \tag{32}$$

At the inclined bottom plate $y = 0$,

$$u_0 = v_0 = 0, \tag{33}$$

$$\frac{\partial \phi_0}{\partial y} = 0. \tag{34}$$

At the inclined top plate $y = d$,

$$\varphi_{20} = 0. \tag{35}$$

At the free surface $y = h(x,t)$,

$$\frac{\partial u_0}{\partial y} = 0, \tag{36}$$

$$\overline{p}_\mathrm{a} - p_0 = \frac{1}{Ca'}\frac{\partial^2 h}{\partial x^2} + \frac{E}{(h-d)^2}, \tag{37}$$

$$\frac{\partial h}{\partial t} + u_0\frac{\partial h}{\partial x} - v_0 = 0, \tag{38}$$

$$\varphi_{20} = 1. \tag{39}$$

Solving the system of equations yields the solution to the zeroth-order equation

$$u_0 = 3\frac{F_\rho}{F_\mu}\left(hy - \frac{1}{2}y^2\right), \tag{40}$$

$$v_0 = -\frac{3}{2}\frac{F_\rho}{F_\mu}\frac{\partial h}{\partial x}y^2, \tag{41}$$

$$p_0 = 3F_\rho \cot\beta (h-y) + \overline{p}_\mathrm{a} - \frac{1}{Ca'}\frac{\partial^2 h}{\partial x^2} - \frac{E}{(h-d)^2}, \tag{42}$$

$$\varphi_{20} = \frac{y-d}{h-d}. \tag{43}$$

Similarly, we can obtain the first-order governing equations and boundary conditions

$$\frac{\partial u_1}{\partial x} + \frac{\partial v_1}{\partial y} = 0, \tag{44}$$

$$Re\left(\frac{\partial u_0}{\partial t} + u_0\frac{\partial u_0}{\partial x} + v_0\frac{\partial u_0}{\partial y}\right) = -\frac{\partial p_0}{\partial x} + F_\mu\frac{\partial^2 u_1}{\partial y^2}, \tag{45}$$

$$-\frac{\partial p_1}{\partial y} + F_\mu\frac{\partial^2 v_0}{\partial y^2} = 0, \tag{46}$$

$$\frac{\partial \phi_1}{\partial t} + u_1\frac{\partial \phi_1}{\partial x} + v_1\frac{\partial \phi_1}{\partial y} = 0. \tag{47}$$

At the inclined bottom plate $y = 0$,

$$u_1 = v_1 = 0, \tag{48}$$

$$\frac{\partial \phi_1}{\partial y} = 0. \tag{49}$$

At the free surface $y = h(x,t)$,

$$\frac{\partial u_1}{\partial y} = 0, \tag{50}$$

$$-p_1 + 2F_\mu\left(\frac{\partial v_0}{\partial y} - \frac{\partial u_0}{\partial y}\frac{\partial h}{\partial x}\right) = 0, \tag{51}$$

$$\frac{\partial h}{\partial t} + u_1\frac{\partial h}{\partial x} - v_1 = 0. \tag{52}$$

Solving the system of equations yields the solution to the first-order equation

$$\begin{aligned} u_1 \;=\; & Re\frac{F_\rho}{{F_\mu}^2}\left[\frac{1}{2}\left(y^3 - 3h^2y\right)\frac{\partial h}{\partial t} + \frac{F_\rho}{F_\mu}\frac{3}{8}\left(hy^4 - 4h^4y\right)\frac{\partial h}{\partial x}\right] \\ & + \frac{F_\rho}{F_\mu}\frac{3}{2}\left(y^2 - 2hy\right)\cot\beta\frac{\partial h}{\partial x} \\ & + \frac{1}{F_\mu}\frac{1}{Ca'}\left(hy - \frac{1}{2}y^2\right)\frac{\partial^3 h}{\partial x^3} \\ & + \frac{1}{F_\mu}\frac{E}{(h-d)^3}\left(y^2 - 2hy\right)\frac{\partial h}{\partial x}. \end{aligned} \tag{53}$$

From the continuity equation, we have

$$\frac{\partial h}{\partial t} = -3\frac{F_\rho}{F_\mu}h^2\frac{\partial h}{\partial x}. \tag{54}$$

Substituting Eq. (54) into Eq. (53), we obtain

$$\begin{aligned} u_1 \;=\; & Re\frac{F_\rho^2}{F_\mu^3}\frac{3}{8}\left(hy^4 - 4h^2y^3 + 8h^4y\right)\frac{\partial h}{\partial x} \\ & + \frac{F_\rho}{F_\mu}\frac{3}{2}\left(y^2 - 2hy\right)\cot\beta\frac{\partial h}{\partial x} \\ & + \frac{1}{F_\mu}\frac{1}{Ca'}\left(hy - \frac{1}{2}y^2\right)\frac{\partial^3 h}{\partial x^3} \\ & + \frac{1}{F_\mu}\frac{E}{(h-d)^3}\left(y^2 - 2hy\right)\frac{\partial h}{\partial x}. \end{aligned} \tag{55}$$

The local flow rate $q(x,t)$ is defined as

$$q(x,t) = \int_0^h u(x,y,t)\,\mathrm{d}y, \tag{56}$$

where $u(x,y,t)=u_0(x,y,t)+\alpha u_1(x,y,t)+O(\alpha^2)$. By solving the integral on the right side, we get

$$q(x,t) = \frac{F_\rho}{F_\mu}h^3+\alpha\left[Re\frac{F_\rho^2}{F_\mu^3}\frac{6}{5}h^6\frac{\partial h}{\partial x}-\frac{F_\rho}{F_\mu}\cot\beta h^3\frac{\partial h}{\partial x} + \frac{1}{F_\mu}\frac{1}{3Ca'}h^3\frac{\partial^3 h}{\partial x^3}-\frac{1}{F_\mu}\frac{E}{(h-d)^3}\frac{2}{3}h^3\frac{\partial h}{\partial x}\right]. \quad (57)$$

By employing an alternative form of the kinematic boundary condition

$$\frac{\partial h}{\partial t}+\frac{\partial q}{\partial x}+O\left(\alpha^2\right)=0. \quad (58)$$

We obtain a nonlinear evolution equation for the thickness of the film

$$h_t+A(h)h_x+\alpha(B(h)h_x+C(h)h_{xxx})_x=0, \quad (59)$$

where,

$$A(h)=\frac{F_\rho}{F_\mu}3h^2, \quad (60)$$

$$B(h)=Re\frac{F_\rho^2}{F_\mu^3}\frac{6}{5}h^6-\frac{F_\rho}{F_\mu}\cot\beta h^3-\frac{1}{F_\mu}\frac{E}{(h-d)^3}\frac{2}{3}h^3, \quad (61)$$

$$C(h)=\frac{1}{F_\mu}\frac{1}{3Ca'}h^3. \quad (62)$$

The physical property parameters of the nanofluid are given by the following formulas:[47,48]

$$F_\mu=\frac{\mu_{\rm n}}{\mu_{\rm f}}=(1-\phi_{\rm ave}\phi)^{-2.5},\quad F_\rho=\frac{\rho_{\rm n}}{\rho_{\rm f}}=1+\zeta\phi_{\rm ave}\phi, \quad (63)$$

where the coefficient $\zeta=\rho_{\rm n}/\rho_{\rm f}-1$ represents the normal density difference between the nanoparticles and the base fluid. Given that most types of nanoparticles are heavier than common base fluids, we consider the value of ζ in this article to be within the range of [0, 5].

4. Linear stability analysis

To study the stability of film flow, a small perturbation at the free surface is assumed. The film thickness h under the perturbed state can be written as

$$h=1+\eta(x,t), \quad (64)$$

where $\eta\ll 1$ represents the dimensionless thickness of the film in the absence of perturbation.

To eliminate the α in Eq. (59), we set the conversion

$$x=\alpha\widetilde{x},\quad t=\alpha\widetilde{t}. \quad (65)$$

By substituting Eqs. (64) and (65) into Eq. (59), retaining up to $O(\eta^3)$, after dropping the cap sign, we obtain

$$\eta_t+A_1\eta_x+B_1\eta_{xx}+C_1\eta_{xxxx}+A_1'\eta\eta_x +B_1'\left(\eta\eta_{xx}+\eta_x^2\right)+C_1'\left(\eta\eta_{xxxx}+\eta_x\eta_{xxx}\right) +\frac{1}{2}A_1''\eta^2\eta_x+B_1''\left(\frac{1}{2}\eta^2\eta_{xx}+\eta\eta_x^2\right) +C_1''\left(\frac{1}{2}\eta^2\eta_{xxxx}+\eta\eta_x\eta_{xxx}\right)+O(\eta^4)=0, \quad (66)$$

where A_1, B_1, C_1, and their corresponding derivatives (denoted by primes) are the values corresponding to $h=1$. To study the linear response of the film, we assume the form of perturbation to be a sinusoidal disturbance, that is

$$\eta(x,t)=\Gamma\exp[{\rm i}(kx-\omega t)]+{\rm c.c.}, \quad (67)$$

where Γ is the amplitude of the disturbance, c.c. is the complex conjugate, k is the wave number. And $\omega=\omega_{\rm r}+{\rm i}\omega_{\rm i}$ is the complex frequency, $\omega_{\rm r}$ and $\omega_{\rm i}$ are the linear growth rates of oscillation frequency and amplitude, respectively. By substituting Eq. (67) into Eq. (66) and considering the linear part, the dispersion relation can be obtained as

$${\rm Disp}(\omega,k)=-{\rm i}\omega+{\rm i}A_1k-B_1k^2+C_1k^4=0. \quad (68)$$

In Eq. (68), the real and the imaginary parts of ω are expressed as

$$\omega_{\rm r}=A_1k, \quad (69)$$

$$\omega_{\rm i}=B_1k^2-C_1k^4. \quad (70)$$

If the linear growth rate of the amplitude $\omega_{\rm i}=0$, the flow is said to be neutrally stable. At this point, the critical Reynolds number is obtained as

$$Re_{\rm c}=\frac{F_\mu^2}{F_\rho}\frac{5}{6}\cot\beta+\left(\frac{F_\mu}{F_\rho}\right)^2\frac{5}{9}\frac{E}{(h-d)^3}. \quad (71)$$

When we consider the relative density and relative viscosity of the nanofluid to be 1, and the electric field to be 0, that is, $F_\rho=F_\mu=1$ and $E=0$, we obtain the critical Reynolds number $Re_{\rm c}=5\cot\beta/6$, which is consistent with existing results.[1,2]

5. Weakly nonlinear analysis

To characterize the nonlinear properties of the thin film flow, we utilize a multiscale approach by expanding the interfacial perturbation η in the form[49,50]

$$\eta(x,x_1,\ldots,t,t_1,t_2,\ldots)=\varepsilon\eta_1+\varepsilon^2\eta_2+\varepsilon^3\eta_3+\cdots, \quad (72)$$

where

$$x_1=\varepsilon x,\quad t_1=\varepsilon t,\quad t_2=\varepsilon^2 t,\quad \ldots, \quad (73)$$

here x and t denote the rapidly varying scales, while x_1, t_1, and so on represent the slowly varying scales. Assuming these

variables are independent of each other, the derivatives with respect to time and space transform as illustrated below:

$$\partial_t \to \partial_t + \varepsilon\partial_{t_1} + \varepsilon^2\partial_{t_2}, \tag{74}$$

$$\partial_x \to \partial_x + \varepsilon\partial_{x_1}. \tag{75}$$

Inserting Eqs. (72)–(75) into Eq. (66), the equation can be obtained as

$$\begin{aligned}&(L_0+\varepsilon L_1+\varepsilon^2 L_2+\cdots)(\varepsilon\eta_1+\varepsilon^2\eta_2+\varepsilon^3\eta_3+\cdots)\\ =\ &-\varepsilon^2 N_2-\varepsilon^3 N_3-\cdots,\end{aligned} \tag{76}$$

where the operators L_0, L_1, L_2, and the nonlinear terms N_2, N_3 in Eq. (76) are expressed as follows:

$$\begin{aligned}
L_0 &= \frac{\partial}{\partial t}+A_1\frac{\partial}{\partial x}+B_1\frac{\partial^2}{\partial x^2}+C_1\frac{\partial^4}{\partial x^4},\\
L_1 &= \frac{\partial}{\partial t_1}+A_1\frac{\partial}{\partial x_1}+2B_1\frac{\partial^2}{\partial x\partial x_1}+4C_1\frac{\partial^4}{\partial x^3\partial x_1},\\
L_2 &= \frac{\partial}{\partial t_2}+B_1\frac{\partial^2}{\partial x_1^2}+6C_1\frac{\partial^4}{\partial x^2\partial x_1^2},\\
N_2 &= A'\eta_1\frac{\partial\eta_1}{\partial x}+B_1'\left[\eta_1\frac{\partial^2\eta_1}{\partial x^2}+\left(\frac{\partial\eta_1}{\partial x}\right)^2\right]\\
&\quad +C_1'\left[\eta_1\frac{\partial^4\eta_1}{\partial x^4}+\frac{\partial\eta_1}{\partial x}\frac{\partial^3\eta_1}{\partial x^3}\right],\\
N_3 &= A_1'\left[\eta_1\left(\frac{\partial\eta_2}{\partial x}+\frac{\partial\eta_1}{\partial x_1}\right)+\eta_2\frac{\partial\eta_1}{\partial x}\right]\\
&\quad +B_1'\left[\eta_1\left(\frac{\partial^2\eta_2}{\partial x^2}+2\frac{\partial^2\eta_1}{\partial x\partial x_1}\right)+\eta_2\frac{\partial^2\eta_1}{\partial x^2}\right.\\
&\quad \left.+2\frac{\partial\eta_1}{\partial x}\left(\frac{\partial\eta_2}{\partial x}+\frac{\partial\eta_1}{\partial x_1}\right)\right]\\
&\quad +C_1'\left[\eta_1\left(\frac{\partial^4\eta_2}{\partial x^4}+4\frac{\partial^4\eta_1}{\partial x^3\partial x_1}\right)+\eta_2\frac{\partial^4\eta_1}{\partial x^4}+\frac{\partial\eta_1}{\partial x}\right.\\
&\quad \left.\times\left(\frac{\partial^3\eta_2}{\partial x^3}+3\frac{\partial^3\eta_1}{\partial x^2\partial x_1}\right)+\frac{\partial^3\eta_1}{\partial x^3}\left(\frac{\partial\eta_1}{\partial x_1}+\frac{\partial\eta_2}{\partial x}\right)\right]\\
&\quad +\frac{1}{2}A_1''\eta_1^2\frac{\partial\eta_1}{\partial x}+B_1''\left[\frac{1}{2}\eta_1^2\frac{\partial^2\eta_1}{\partial x^2}+\eta_1\left(\frac{\partial\eta_1}{\partial x}\right)^2\right]\\
&\quad +C_1''\left[\frac{1}{2}\eta_1^2\frac{\partial^4\eta_1}{\partial x^4}+\eta_1\frac{\partial\eta_1}{\partial x}\frac{\partial^3\eta_1}{\partial x^3}\right].
\end{aligned} \tag{77, 78}$$

For the first-order problem $O(\varepsilon)$, we find

$$L_0\eta_1 = 0, \tag{79}$$

it is assumed that the solution has the form

$$\eta_1 = \Gamma(x_1,t_1,t_2)[\exp \mathrm{i}(kx-\omega_\mathrm{r}t)]+\mathrm{c.c.}, \tag{80}$$

where $\Gamma(x_1,t_1,t_2)$ is the complex amplitude and c.c. is the complex conjugates. It is important to note that the solution presented in Eq. (80), obtained from linear stability analysis, differs only in that ω is replaced by ω_r. This modification is due to ω_i being of the order $O(\varepsilon^2)$ near the neutral curve, making the function $\exp(\omega_\mathrm{i}t)$ slowly varying. Consequently, it can be incorporated into $\Gamma(x_1,t_1,t_2)$.[51]

For the second-order problem $O(\varepsilon^2)$ we obtain as

$$L_0\eta_2 = -L_1\eta_1 - N_2. \tag{81}$$

Substituting Eq. (80) into Eq. (81), we get

$$\begin{aligned}
L_0\eta_2 &= -\mathrm{i}\left[\frac{\partial \mathrm{Disp}(\omega_\mathrm{r},k)}{\partial\omega_\mathrm{r}}\frac{\partial\Gamma}{\partial t_1}\right.\\
&\quad \left.-\frac{\partial \mathrm{Disp}(\omega_\mathrm{r},k)}{\partial k}\frac{\partial\Gamma}{\partial x_1}\right]\mathrm{e}^{\mathrm{i}(kx-\omega_\mathrm{r}t)}\\
&\quad -Q_1\Gamma^2\mathrm{e}^{2\mathrm{i}(kx-\omega_\mathrm{r}t)}+\mathrm{c.c.},
\end{aligned} \tag{82}$$

$$\mathrm{Disp}(\omega,k) = -\mathrm{i}\omega+\mathrm{i}A_1k-B_1k^2+C_1k^4=0, \tag{83}$$

$$Q_1 = \mathrm{i}A_1'k-2B_1'k^2+2C_1'k^4.$$

We eliminate the secular term produced by the first term on the right-hand side of Eq. (82), the solution of Eq. (82) can ultimately be expressed as

$$\eta_2 = -\frac{Q_1\Gamma^2\mathrm{e}^{2\mathrm{i}(kx-\omega_\mathrm{r}t)}}{\mathrm{Disp}(2\omega_\mathrm{r},2k)}+\mathrm{c.c.} \tag{84}$$

By introducing the coordinate transformation $\delta = (x_1 - c_\mathrm{g}t_1)$, where $c_\mathrm{g} = (-\mathrm{Disp}_k/\mathrm{Disp}_{\omega_\mathrm{r}})$, and using the solvability condition of the third-order equation, we obtain

$$\frac{\partial\Gamma}{\partial t_2}+J_1\frac{\partial^2\Gamma}{\partial\delta^2}-\varepsilon^{-2}\omega_\mathrm{i}\Gamma+(J_2+\mathrm{i}J_3)|\Gamma|^2\Gamma=0, \tag{85}$$

where

$$J_1 = B_1-6C_1k^2, \tag{86}$$

$$\begin{aligned}
J_2 &= \frac{1}{2}\left(C_1''k^4-B_1''k^2\right)\\
&\quad +\frac{(A_1')^2k^2+2\left(7C_1'k^4-B_1'k^2\right)\left(B_1'k^2-C_1'k^4\right)}{16C_1k^4-4B_1k^2},
\end{aligned} \tag{87}$$

$$J_3 = \frac{1}{2}A_1''k+\frac{A_1'k\left(B_1'k^2-7C_1'k^4\right)+2A_1'k\left(B_1'k^2-C_1'k^4\right)}{16C_1k^4-4B_1k^2}. \tag{88}$$

Ignoring the diffusion effect of the second term in Eq. (85), we get

$$\frac{\partial\Gamma}{\partial t_2}-\varepsilon^{-2}\omega_\mathrm{i}\Gamma+(J_2+\mathrm{i}J_3)|\Gamma|^2\Gamma=0. \tag{89}$$

It is assumed that the solution of Eq. (89) can be written as

$$\Gamma = a\exp[-\mathrm{i}b(t_2)t_2]. \tag{90}$$

Substituting Eq. (90) into Eq. (89), we get

$$\frac{\partial a}{\partial t_2} = \left(\varepsilon^{-2}\omega_\mathrm{i}-J_2a^2\right)a, \tag{91}$$

$$\frac{\partial[b(t_2)t_2]}{\partial t_2} = J_3a^2. \tag{92}$$

The second term on the right-hand side of Eq. (91) represents a nonlinear term that controls the exponential variation of the linear perturbation, contingent upon the sign of ω_i and

J_2. When the right side of Eq. (91) equals 0, the equilibrium amplitude can be given by

$$\varepsilon a = \sqrt{\frac{\omega_{\mathrm{i}}}{J_2}}. \tag{93}$$

When $J_2 > 0$, the amplitude reaches a saturation point, indicating stability. Conversely, when $J_2 < 0$, the amplitude fails to develop, signifying that $J_2 < 0$ leads to the system's instability. Based on the indicators ω_{i} and J_2, four nonlinear regions are delineated: the supercritical stable region I ($\omega_{\mathrm{i}} > 0, J_2 > 0$), the subcritical unstable region II ($\omega_{\mathrm{i}} < 0, J_2 < 0$), the unconditional stable region III ($\omega_{\mathrm{i}} < 0, J_2 > 0$), and the explosive state region IV ($\omega_{\mathrm{i}} > 0, J_2 < 0$).

6. Numerical simulations

To comprehend the development of disturbances with finite amplitude, we solve the nonlinear evolution Eq. (59) within a periodic domain. This is accomplished by applying the Fourier transform to convert the spatial variables into a series of wave numbers, thereby transforming the problem into a set of ordinary differential equations. The fast Fourier transform algorithm then computes these wave numbers, thereby providing the numerical solution to the nonlinear evolution Eq. (59).[52]

To perform a Fourier transform of the nonlinear evolution equation within the domain x

$$\begin{aligned}\frac{\partial \hat{h}}{\partial t} =& -\mathrm{i}k\cdot F\left\{\frac{F_\rho}{F_\mu}F^{-1}[\hat{h}]^3+\frac{F_\rho^2}{F_\mu^3}Re\frac{6}{5}F^{-1}[\hat{h}]^6F^{-1}[\mathrm{i}k\hat{h}]\right.\\ &-\frac{F_\rho}{F_\mu}\cot\beta F^{-1}[\hat{h}]^3F^{-1}[\mathrm{i}k\hat{h}]\\ &-\frac{1}{F_\mu}\frac{E}{\left(F^{-1}[\hat{h}]-d\right)^3}\frac{2}{3}F^{-1}[\hat{h}]^3F^{-1}[\mathrm{i}k\hat{h}]\\ &\left.+\frac{1}{F_\mu}\frac{1}{3Ca'}F^{-1}[\hat{h}]^3F^{-1}[(\mathrm{i}k)^3\hat{h}]\right\}.\end{aligned} \tag{94}$$

We use perturbations at the most unstable wave number k_{m} as the initial condition and it is given as

$$h(x,0) = 1 + 0.05\cos k_{\mathrm{m}}x. \tag{95}$$

This methodology is adopted because the most unstable wave number is the one that, under specific conditions, accelerates the growth of disturbances on the surface of the liquid film. The most unstable wave number k_{m} is determined by solving $\mathrm{d}\omega_{\mathrm{i}}/\mathrm{d}k = 0$. Consequently, using the perturbation at the least stable wave number k_{m} as the initial condition more accurately represents the system's dynamic behavior, thereby enhancing both the accuracy and stability of the numerical solution.

7. Results and discussion

In the previous section, we derived the nonlinear evolution equations of the interface based on the long-wave assumption and asymptotic expansion. We then solved the dispersion relation via linear stability analysis and carried out a weakly nonlinear analysis using the multiscale method to elucidate various instability mechanisms. In practical engineering contexts, the physical parameters are set as follows. The nanoparticle volume fraction is within the range $0.01 \le \phi \le 0.05$; the liquid density is $\rho_{\mathrm{f}} \approx 1000\ \mathrm{kg/m^3}$; the dynamic viscosity of the base liquid is $\mu_{\mathrm{f}} \approx 10^{-3}\ \mathrm{Pa\cdot s}$; and the viscosity of nanoparticles is approximately $\mu_{\mathrm{n}} \approx (1\text{–}10)\times 10^{-3}\ \mathrm{Pa\cdot s}$ depending on particle type and concentration. The surface tension is set as $\sigma_0 \approx 0.072\ \mathrm{N/m}$; the applied electric potential is assumed to be $\varphi_{\mathrm{c}} \approx 10^{-1}$ V–10^2 V, corresponding to an estimated local electric field strength of $E_{\mathrm{c}} \approx 10^4$ V/m–10^6 V/m based on the characteristic length scale; the initial film thickness is taken as $h_0 \approx 10^{-4}$ m–10^{-3} m; and the characteristic velocity is $U_0 \approx 0.01$ m/s–0.1 m/s.[53–56]

Using these parameters, we estimate the key dimensionless groups as follows: the Reynolds number is $Re = \frac{\rho_{\mathrm{f}}U_0h_0}{\mu_{\mathrm{f}}} \approx$ 1–100; the modified capillary number is defined as $Ca' = \mu_{\mathrm{f}}U_0/\alpha^2\sigma_0$, where α is the long-wave expansion parameter (typically $\alpha \approx 0.01$–0.1), leading to an estimated range of $Ca' \approx 10^{-3}$–10^{-1}; and the dimensionless electric field parameter is expressed as $E = \varepsilon_0\varphi_{\mathrm{c}}^2/2\mu_{\mathrm{f}}U_0h_0$, where $\varepsilon_0 = 8.854\times 10^{-12}$ F/m, giving $E \approx 10^{-2}$–10^2. In the following section, we adopt representative values of these parameters according to actual operating conditions in engineering systems to further interpret the results and provide a theoretical basis for application. Furthermore, the Fourier spectral method is employed to visualize the evolution of the interface.

7.1. Linear stability analysis

Figure 2 illustrates the temporal growth rate curves for various values of the electric parameter E, based on the linear dispersion relation $\omega_{\mathrm{i}} = B_1k^2 - C_1k^4$. As shown, the growth rate ω_{i} initially increases with the wavenumber k and then decreases, forming a peak that indicates the most unstable mode. It is evident that the peak value of ω_{i} rises with increasing E, indicating that a stronger electric field enhances the instability of the flow. This destabilizing effect stems primarily from the normal Maxwell stress induced at the liquid–air interface. The presence of an electric field generates an electrostatic pressure jump across the interface due to dielectric contrast, which modifies the interfacial normal stress balance. When surface perturbations occur, this normal stress varies along the interface and reinforces the perturbation, thereby promoting instability. In such thin film systems, where surface forces dom-

inate, the destabilizing contribution of the electric field becomes particularly significant.[44]

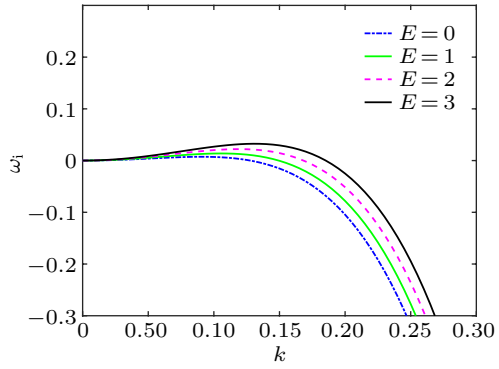


Fig. 2. Temporal growth rate curve derived from $\omega_i = B_1k^2 - C_1k^4$ for different values of electric parameter when $Re = 2$, $\beta = \pi/3$, $d = 2$, $\phi = 0.05$, $\zeta = 2$.

Figure 3 illustrates the temporal growth rate curves for various values of nanoparticle volume fraction ϕ, based on the linear dispersion relation $\omega_i = B_1k^2 - C_1k^4$. It is evident that as ϕ increases, the peak value of ω_i decreases, indicating a stabilizing effect of nanoparticles on the flow. This stabilization can be attributed to the viscosity-enhancing nature of nanoparticles. The inclusion of nanoparticles increases the effective viscosity of the nanofluid, thereby damping out velocity gradients and suppressing the growth of interfacial disturbances. As viscous dissipation becomes more dominant, energy input from perturbations is more effectively absorbed, resulting in a reduced instability growth rate.

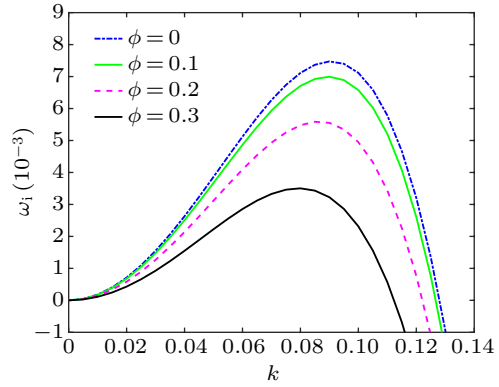


Fig. 3. Temporal growth rate curve derived from $\omega_i = B_1k^2 - C_1k^4$ for different values of nanoparticle volume fraction when $Re = 2$, $\beta = \pi/3$, $d = 2$, $E = 0$, $\zeta = 2$.

Figure 4 presents the temporal growth rate curves for various values of the normal density difference ζ between the nanoparticles and the base fluid. The results show that increasing ζ enhances the growth rate ω_i, signifying a destabilizing effect. This destabilization arises due to the density stratification introduced by ζ, which amplifies gravitational body force differences in the fluid layer. When the denser nanoparticles tend to settle more strongly under gravity, they enhance the buoyancy-driven imbalance in the perturbed regions, which in turn increases the growth of disturbances. This mechanism is further supported by the observation that the critical Reynolds number Re_c decreases with increasing ζ (see Fig. 5), indicating a lowered threshold for the onset of instability.

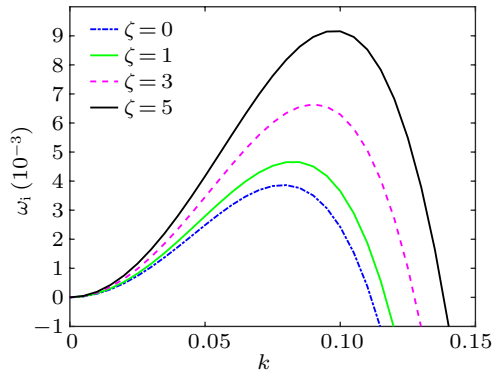


Fig. 4. Temporal growth rate curve derived from $\omega_i = B_1k^2 - C_1k^4$ for different values of normal density difference when $Re = 2$, $\beta = \pi/3$, $d = 2$, $E = 0$, $\phi = 0.2$.

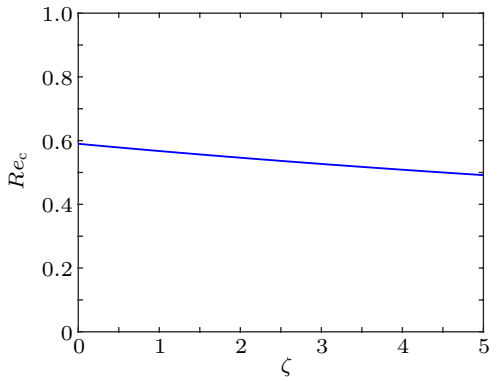


Fig. 5. Critical Reynolds number changes with the normal density difference when $\beta = \pi/3$, $d = 2$, $E = 0$, $\phi = 0.2$.

7.2. Weakly nonlinear stability analysis

Figure 6 presents the stability diagram with wave number k plotted against Reynolds number Re for various values of the electric field parameter E. It is observed that as E increases, the subcritical instability region II and the unconditionally stable region III gradually contract, while the supercritical stable region I and the explosive region IV expand. Moreover, the critical Reynolds number Re_c decreases with increasing E, indicating that the flow becomes unstable at lower flow rates. This destabilization arises from the normal Maxwell stress generated by the electric field at the liquid–air interface, which enhances interfacial deformation and promotes instability of the liquid film.

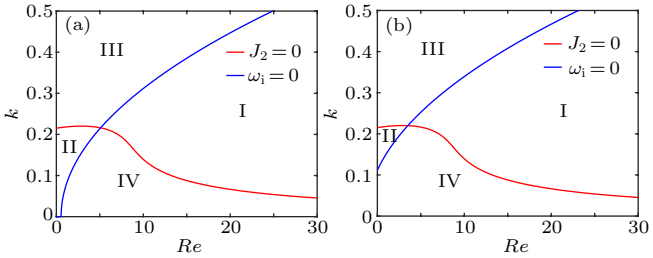


Fig. 6. Stability curves, (a) $E = 0$, (b) $E = 3$, for different electrical parameters when $\beta = \pi/3$, $d = 2$, $\phi = 0.2$, $\zeta = 2$.

Figure 7 illustrates the correlation between the wave number k and Reynolds number Re for varying volume fractions of nanoparticles ϕ. The study reveals that under the same conditions, both subcritical instability region II and unconditionally stable region III expand with an increase in ϕ. Conversely, the supercritical stable region I and the explosive state region IV diminish. Additionally, the critical Reynolds number Re_c escalates as the volume fraction of nanoparticles ϕ rises. Consequently, the presence of nanoparticles suppresses the instability of the liquid film flow.

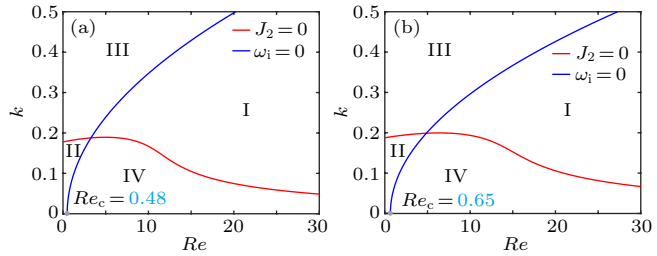


Fig. 7. Stability curves, (a) $\phi=0$, (b) $\phi=0.3$, for different volume fractions of nanoparticles when $\beta=\pi/3$, $d=2$, $E=0$, $\zeta=2$.

In Fig. 8, we depict the stability curves of wave number k as they vary with Reynolds number Re for different standard density differences ζ. It is evident that the critical Reynolds number Re_c diminishes as the normal density difference ζ escalates. For instance, in Fig. 8(a), $Re_c=0.49$, whereas in Fig. 8(b), $Re_c=0.59$. Additionally, the subcritical instability region II and the unconditionally stable region III shrink, while the supercritical stable region I and the explosive state region IV expand. Hence, the standard density difference between nanoparticles and the base fluid enhances the instability of the flow.

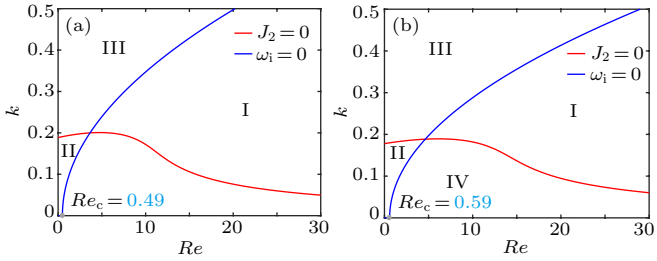


Fig. 8. Stability curves, (a) $\zeta=5$, (b) $\zeta=0$, for different normal density differences when $\beta=\pi/3$, $d=2$, $E=0$, $\phi=0.2$.

7.3. Numerical simulations

Figures 9 and 10 illustrate the short-term evolution of the free surface within the supercritical region for various values of the electrical parameter E and the normal density difference ζ, respectively. Within the timeframe of $t=0.1$ to $t=1$, the disturbance amplitudes increase progressively, indicating the onset and amplification of liquid film instability. The amplitude peaks are more pronounced at higher values of E and ζ, which is consistent with the destabilizing effects identified in the linear and weakly nonlinear stability analyses. Specifically, the electric field induces a normal Maxwell stress at the liquid–air interface, amplifying surface deformations and promoting instability. Similarly, a larger density difference ζ enhances gravitational forces acting on the interface, accelerating disturbance growth and destabilizing the film.

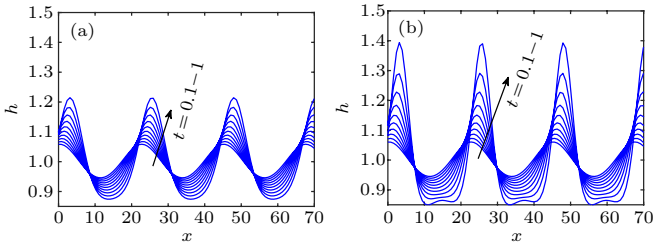


Fig. 9. Film thickness at different times, (a) $E=0$, (b) $E=5$, when $Re=20, \beta=\pi/3, d=2, \phi=0.05, \zeta=2$.

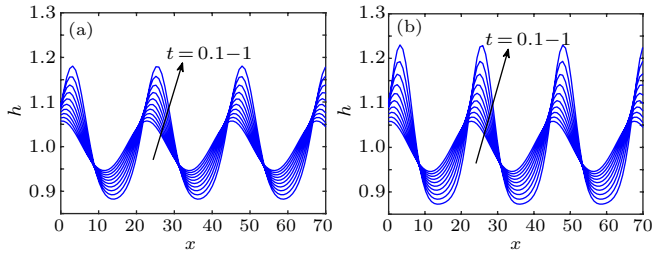


Fig. 10. Stability curves, (a) $\zeta=0$, (b) $\zeta=4$, when $Re=20$, $\beta=\pi/3$, $d=2$, $E=0$, $\phi=0.1$.

Figure 11 depicts the short-term evolution of the free surface under varying nanoparticle volume fractions ϕ within the same supercritical regime. The results show that while disturbances still grow over time, the peak amplitudes decrease as ϕ increases. This reflects a stabilizing effect exerted by the nanoparticles. The enhanced viscosity of the nanofluid due to a higher volume fraction ϕ increases internal dissipation, suppressing the growth of surface perturbations and thus delaying the onset of instability.

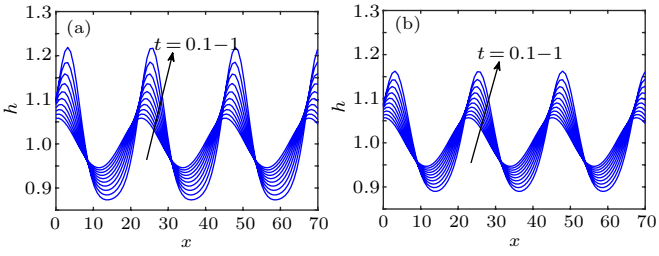


Fig. 11. Stability curves, (a) $\phi=0$, (b) $\phi=0.2$, when $Re=20, \beta=\pi/3, d=2, E=0, \zeta=2$.

8. Conclusion

This study investigates the instability of nanofluid film flow along an inclined surface under the influence of an electric field. By deriving a nonlinear evolution equation and conducting both linear and weakly nonlinear stability analyses,

supplemented by numerical simulations, we reveal the physical mechanisms underlying the instability behavior. The results show that the electric field exerts a destabilizing effect on the liquid film. This arises from the electrostatic pressure gradient formed at the fluid interface, which generates Maxwell stresses that amplify initial perturbations. In thin-film systems, such interfacial electric forces are especially prominent, resulting in enhanced instability. In contrast, the volume fraction of the nanoparticles exhibits a stabilizing effect. A higher volume fraction increases the effective viscosity of the nanofluid, leading to a stronger viscous dissipation that suppresses perturbation growth. Moreover, interparticle interactions may produce microstructural effects that further stabilize the interface. However, the density difference between nanoparticles and the base fluid enhances instability, as it induces a vertical density gradient under gravity, promoting Rayleigh–Taylor-like instabilities.

In examining weakly nonlinear stability, we classify the system into four regions according to the signs of the imaginary part of the growth rate, ω_{i}, and the Landau coefficient, J_2. It is observed that increasing the electric field strength E and the normal density difference ζ leads to a shrinkage of the subcritical instability region (region II) and the unconditionally stable region (region III), while the supercritical stable region (region I) and the explosive instability region (region IV) expand. This indicates that both E and ζ promote nonlinear instability and reduce the parameter space in which the system remains stable. In contrast, increasing the nanoparticle volume fraction ϕ has the opposite effect, suppressing instability and expanding the stable regions, which is consistent with its viscous damping role.

Finally, to further understand the nonlinear evolution of the interface, we numerically solved the nonlinear evolution equation by using the fast Fourier transform method. The simulation results are in good agreement with the predictions from the linear stability analysis. In the unstable regime, the perturbation amplitude grows continuously over time, leading to significant interface deformation. This confirms that the electric field and the density difference play dominant roles in destabilizing the nanofluid film, while the nanoparticle volume fraction acts to mitigate such the instability through enhanced viscous effects.

Appendix A: Matlab code for solving Eq. (94)

```
clear;
global beta Ca Re E f zeta
beta = pi/3; Ca = 0.003; Re = 20;
E = 5; f = 0.05; zeta = 2;

% Parameter settings
L = 14 * pi / 0.28; % Spatial domain length
N = 200; % Number of grid points
x = L / N * (-N/2:N/2-1); % Spatial coordinates (periodic domain)
k = 2 * pi / L * [0:N/2-1 -N/2:-1].'; % Fourier space wavenumbers

% Initial condition
h0 = 1 + 0.05 * cos(0.28 * x); % Initial perturbation (periodic disturbance)
ht0 = fft(h0); % Fourier transform ofthe initial condition

% Time integration
tspan = [0 1]; % Time span for integration
[t, htsol] = ode45(@(t, ht) film_fun(t, ht, k), tspan, ht0); % Solve ODE system
hsol = ifft(htsol, [], 2); % Inverse Fourier transform to get h(x,t)

% Plot the result
plot(x, real(hsol(end,:)), 'b'); % Plot the real part at final time
axis([0 70 0.85 1.3])
xlabel('x');
ylabel('h');
hold on

% ---------- Function Definition: RHS of Evolution Equation ---------- %
function dht = film_fun(~, ht, k)
    % Parameter settings
    global beta Ca Re E f zeta

    % Pre-factors (constant coefficients)
    F1 = (1 - f^2)^(-2.5);
    F2 = 1 + zeta * f^2;

    % Inverse Fourier transform to get h(x,t)
    h = ifft(ht);


    % Construct the right-hand side (RHS) terms
    % Each term corresponds to a physical effect (refer to derivation)
    nonlin1 = (F2 / F1) * h.^3;
    nonlin2 = (Re / F1) * (F2 / F1)^2 * (6/5) * h.^6 .* ifft(1i * k .* ht);
    nonlin3 = -(F2 / F1) * cot(beta) * h.^3 .* ifft(1i * k .* ht);
    elecTerm = -(1 / F1) * E * (1 ./ (h - 2)).^3 * (2/3) .* h.^3 .* ifft(1i * k .* ht);
    capTerm = (1 / F1) * (1 / (3 * Ca)) * h.^3 .* ifft((1i * k).^3 .* ht);

    % Total time derivative in Fourier space
    dht = -1i * k .* fft(nonlin1 + nonlin2 + nonlin3 + elecTerm + capTerm);
end
```

Acknowledgements

Project supported by the National Natural Science Foundation of China (Grant Nos. 11902165, 12272188, 12102205, and 12262025), the National Science Foundation for Distinguished Young Scholars of the Inner Mongolia Autonomous Region of China (Grant No. 2023JQ16), the Program for Young Talents of Science and Technology in Universities of Inner Mongolia Autonomous Region (Grant No. NJYT23098), and the Scientific Startin and the Innovative Research Team in Universities of Inner Mongolia Autonomous Region of China (Grant No. NMGIRT2208).

References

[1] Benjamin T B 1957 *J. Fluid Mech.* **2** 554
[2] Yih C S 1955 *Q. Appl. Math.* **12** 434
[3] Yih C S 1969 *Fluid Mechanics: A Concise Introduction to the Theory* (McGraw-HilleBooks)

[4] Oron A, Davis S H and Bankoff S G 1997 *Rev. Mod. Phys.* **69** 931
[5] Kalliadasis S, Kiyashko A and Demekhin E A 2003 *J. Fluid Mech.* **475** 377
[6] Tseluiko D and Papageorgiou D T 2006 *J. Fluid Mech.* **556** 361
[7] Thiele U, Goyeau B and Velarde M G 2009 *Phys. Fluids* **21** 014103
[8] Hu K X, He M and Chen Q S 2016 *Phys. Fluids* **28** 033105
[9] Hu K X, He M, Chen Q S and Liu R 2017 *Phys. Fluids* **29** 073101
[10] Morad A M, M A S and I E G 2020 *Phys. Scr.* **95** 025205
[11] Hu K X, Zhang S N and Chen Q S 2023 *J. Fluid Mech.* **958** A22
[12] Tian K, Xue C, Cui J, Qin K and Ding Z 2024 *J. Non-Newtonian Fluid Mech.* **333** 105324
[13] Hu K X, Du K and Chen Q S 2024 *J. Fluid Mech.* **999** A14
[14] Liu R and Ding Z 2020 *J. Fluid Mech.* **899** A14
[15] Ding Z and Wong T 2017 *Phys. Fluids* **29** 011701
[16] Chattopadhyay S 2021 *Phys. Fluids* **33** 082102
[17] Samanta A 2020 *Phys. Fluids* **32** 064105
[18] Chen C I, Chen C K and Yang Y T 2003 *Int. J. Eng. Sci.* **41** 1313
[19] Closa F, Ziebert F and Raphael E 2012 *Math. Model. Nat. Phenom.* **7** 6
[20] Wasa K 2012 *Handbook of sputter deposition technology: fundamentals and applications for functional thin films, nano-materials and MEMS* (William Andrew)
[21] Zargar R A 2023 *Metal Oxide Nanocomposite Thin Films for Optoelectronic Device Applications* (John Wiley & Sons)
[22] Kumar A, Verma C and Thakur A 2023 *Corrosion Mitigation Coatings: Functionalized Thin Film Fundamentals and Applications* (Walter de Gruyter GmbH & Co KG)
[23] Benney D J 1966 *J. Math. Phys.* **45** 150
[24] Lin S P 1974 *J. Fluid Mech.* **63** 417
[25] Gjevik B 1970 *Phys. Fluids* **13** 1918
[26] Nakaya C 1975 *Phys. Fluids* **15** 1407
[27] Chang H C 1989 *Phys. Fluids* **1** 1314
[28] Kondic L 2003 *SIAM Rev.* **45** 95
[29] Banerjee D, Souslov A and Abanov A 2017 *Nat. Commun.* **8** 1573
[30] Bauer R J and Kerczek C V 1991 *J. Appl. Mech.* **58** 278
[31] Zhang Y and Ding Z 2023 *Phys. Rev. Fluids* **8** 064001
[32] Sheremet M A, Trimbitas R, Grosan T and Pop I 2018 *Appl. Math. Mech. -Engl. Ed.* **39** 1425
[33] Lin J Z, Xia Y and Ku X K 2016 *Int. J. Heat Mass Transfer* **93** 57
[34] Xiong X P, Chen S and Yang B 2017 *Appl. Math. Mech. Engl. Ed.* **38** 585
[35] Nayak A K, Gartia M R and Vijayan P K 2008 *Exp. Therm. Fluid Sci.* **33** 184
[36] Nayak A K, Gartia M R and Vijayan P K 2009 *Nuc. Eng. Des.* **239** 526
[37] Lin J Z, Xia Y and Bao F B 2014 *Fluid Dyn. Res.* **46** 055512
[38] Dero S, Rohni A M, Saaban A and Khan I 2019 *Energies* **12** 4529
[39] Lin J and Yang H 2019 *Appl. Math. Mech. Engl. Ed.* **40** 1227
[40] Bankoff S G, Griffing E M and Schluter R A 2002 *Ann. N. Y. Acad. Sci.* **974** 1
[41] Griffing E M, Bankoff S G and Miksis M J 2006 *J. Fluids Eng.* **128** 276
[42] Gonzalez A and Castellanos A 1996 *Phys. Rev. E* **53** 3573
[43] Tseluiko D, Blyth M G and Papageorgiou D T 2008 *J. Fluid Mech.* **597** 449
[44] Samanta A 2019 *Phys. Fluids* **31** 034109
[45] Uma B and Usha R 2010 *Phys. Rev. E* **82** 016305
[46] Hatami M and Jing D 2020 *Nanofluids: mathematical, numerical, and experimental analysis* (Academic Press)
[47] Cheng Z and Peng J 2020 *Int. J. Heat Mass Transfer* **146** 118895
[48] Cao Z, Zhao J, Wang Z, Liu F and Zheng L 2016 *J. Mol. Liq.* **222** 1121
[49] Dandapat B S and Mukhopadhyay A 2003 *Int. J. Appl. Mech. Eng.* **8** 379
[50] Mukhopadhyay A and Dandapat B S 2004 *J. Phys. D Appl. Phys.* **38** 138
[51] Mukhopadhyay A, Dandapat B S and Mukhopadhyay A 2008 *Int. J. Non-Linear Mech.* **43** 632
[52] Chattopadhyay S, Subedar G Y, Gaonkar A K, Barua A K and Mukhopadhyay A 2022 *Int. J. Non-Linear Mech.* **140** 103905
[53] Porgar S, Oztop H F and Salehfekr S 2023 *J. Mol. Liq.* **386** 122213
[54] Jia B and Jian Y 2022 *Phys. Fluids* **34** 044104
[55] Wang J, Jia B and Jian Y 2024 *Phys. Fluids* **36** 094101
[56] Verma R, Sharma A, Kargupta K and Bhaumik J 2005 *Langmuir* **21** 3710